Metabolic connectivity mapping reveals effective connectivity in the resting human brain

Valentin Riedl[a,b,c,1], Lukas Utz[a,c,d], Gabriel Castrillón[a,c,e], Timo Grimmer[c,f], Josef P. Rauschecker[c,d,g], Markus Ploner[c,h], Karl J. Friston[i], Alexander Drzezga[j], and Christian Sorg[a,c,f]

[a]Department of Neuroradiology, Klinikum rechts der Isar, Technischen Universitaet Muenchen, 81675 Muenchen, Germany; [b]Department of Nuclear Medicine, Klinikum rechts der Isar, Technischen Universitaet Muenchen, 81675 Muenchen, Germany; [c]Neuroimaging Center, Klinikum Rechts der Isar, Technischen Universitaet Muenchen, 81675 Muenchen, Germany; [d]Institute of Advanced Studies, Technischen Universitaet Muenchen, 81675 Muenchen, Germany; [e]Instituto de Alta Tecnologia Medica, 050026 Medellin, Colombia; [f]Department of Psychiatry and Psychotherapy, Klinikum Rechts der Isar, Technischen Universitaet Muenchen, 81675 Muenchen, Germany; [g]Laboratory of Integrative Neuroscience and Cognition, Georgetown University, Washington, DC 20057; [h]Department of Neurology, Klinikum Rechts der Isar, Technischen Universitaet Muenchen, 81675 Muenchen, Germany; [i]The Wellcome Trust Centre for Neuroimaging, University College London, London WC1N 3BG, United Kingdom; and [j]Department of Nuclear Medicine, Uniklinik Köln, 50937 Köln, Germany

Edited by Peter A. Bandettini, National Institutes of Mental Health, Bethesda, MD, and accepted by the Editorial Board December 4, 2015 (received for review July 13, 2015)

Directionality of signaling among brain regions provides essential information about human cognition and disease states. Assessing such effective connectivity (EC) across brain states using functional magnetic resonance imaging (fMRI) alone has proven difficult, however. We propose a novel measure of EC, termed metabolic connectivity mapping (MCM), that integrates undirected functional connectivity (FC) with local energy metabolism from fMRI and positron emission tomography (PET) data acquired simultaneously. This method is based on the concept that most energy required for neuronal communication is consumed postsynaptically, i.e., at the target neurons. We investigated MCM and possible changes in EC within the physiological range using "eyes open" versus "eyes closed" conditions in healthy subjects. Independent of condition, MCM reliably detected stable and bidirectional communication between early and higher visual regions. Moreover, we found stable top-down signaling from a frontoparietal network including frontal eye fields. In contrast, we found additional top-down signaling from all major clusters of the salience network to early visual cortex only in the eyes open condition. MCM revealed consistent bidirectional and unidirectional signaling across the entire cortex, along with prominent changes in network interactions across two simple brain states. We propose MCM as a novel approach for inferring EC from neuronal energy metabolism that is ideally suited to study signaling hierarchies in the brain and their defects in brain disorders.

simultaneous PET/fMRI | energy metabolism | directional signaling | effective connectivity | resting state

Complex cognition emerges by integrating upstream sensory information with feedback signaling from higher cortical regions (1–4). Networks related to sensory processing or cognition reliably occur in the human brain even at rest (5, 6). These networks are identified by synchronous signal fluctuations, or functional connectivity (FC), among brain regions when neuronal activity is recorded by functional magnetic resonance imaging (fMRI). In recent years, various FC patterns have emerged as reliable indicators of different brain states, because they have been found to adapt to recent behavior or cognition (7–12) and to be disrupted in patients suffering from specific psychiatric disorders (13, 14). Further knowledge about important aspects of cognition and diseases could be gained from a better distinction between feedback and feedforward communication. Our understanding of the signaling hierarchy in different brain states remains incomplete, however.

Although FC captures correlations among neuronal signals, only effective connectivity (EC) describes the influence exerted by one neuronal system over another (15). Recent approaches to modeling EC during different brain states appear promising (16, 17), but face problems inherent to fMRI. First, EC is estimated directly from the time-varying fluctuations or cross-spectra of the observed fMRI signal, and thus is prone to confounds from different hemodynamic responses across groups, particularly when studying patient populations (15, 17). Second, analyses are usually restricted to a limited number of brain regions, owing to the need for complex computations. Here we propose a novel approach integrating FC with simultaneously measured energy metabolism from positron emission tomography (PET) to derive a voxel-wise, whole-brain mapping of EC in humans.

Energy consumption is an essential aspect of neuronal communication. Consistently across species, the greatest amount of energy metabolism is dedicated to signaling, with the remaining part dedicated to housekeeping functions (18). Up to 75% of signaling-related energy is consumed postsynaptically, i.e., at the target neurons (19–22). Scaled to the systems level, we assume that an increase in local metabolism reflects an increase in afferent EC from source regions. We hypothesize that the spatial profile of this relationship is expressed in terms of spatial correlations between metabolic activity and long-range FC, which we term metabolic connectivity mapping (MCM). We simultaneously acquired fMRI and PET data for the glucose analog ^{18}F-fludeoxyglucose (FDG) during two different brain states, as reported previously (10). In individual subject space, we

Significance

Noninvasive brain imaging of humans identifies prominent networks related to sensory and cognitive functions in the resting state; however, the signaling hierarchy and directionality among these networks remain largely unknown. Integrating simultaneously recorded measures for network identification and regional energy metabolism, we propose metabolic connectivity mapping (MCM) as a novel measure to reveal signaling directionality in the human brain. Comparing simple "eyes closed" and "eyes open" conditions in healthy subjects, MCM revealed stable bidirectional signaling among visual cortices and top-down signaling from parietal control regions. Additional top-down signaling from a salience network occurs only during the eyes open condition. We propose MCM as a measure for investigating signaling directions among brain networks in healthy and diseased brains.

Author contributions: V.R., A.D., and C.S. designed research; V.R., T.G., and A.D. performed research; V.R., L.U., and G.C. analyzed data; and V.R., J.P.R., M.P., K.J.F., A.D., and C.S. wrote the paper.

The authors declare no conflict of interest.

This article is a PNAS Direct Submission. P.A.B. is a guest editor invited by the Editorial Board.

Freely available online through the PNAS open access option.

[1]To whom correspondence should be addressed. Email: valentin.riedl@mytum.de.

This article contains supporting information online at www.pnas.org/lookup/suppl/doi:10.1073/pnas.1513752113/-/DCSupplemental.

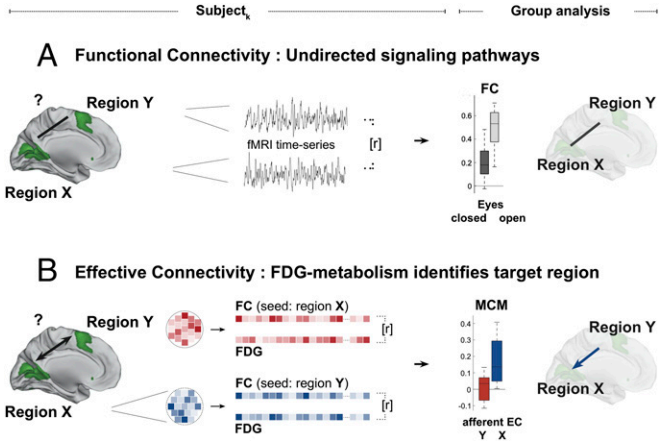

Fig. 1. MCM reveals EC in the human brain. (*A*) FC reveals undirected pathways of synchronous fMRI signal fluctuations between two regions, X and Y. For each subject, FC is calculated as the temporal correlation, [r] between the cluster time series. In our example, we identified FC pathways during conditions of eyes closed and eyes open. (*B*) In a next step, we identified EC (i.e., the directionality of signaling) in a given functional pathway. For each region, we calculated the spatial correlation, [r], between voxel FC and FDG values of simultaneously acquired fMRI and PET data. According to cellular recordings (see text), the majority of signaling-related energy is consumed postsynaptically, i.e., at the target region. Thus, MCM identifies afferent EC in the signaling pathway between region X and region Y.

performed spatial correlation analyses of voxel FC and FDG to test whether the metabolic profile indicates the target area of communication between functionally connected regions (Fig. 1).

Vision is the only sensation that can be interrupted volitionally in a natural way. Opening the eyes is a fundamental behavior for directing attention to the external world, i.e., changing from an interoceptive state to an exteroceptive state (3, 23, 24). Current knowledge of the signaling hierarchy in the extended visual system has emerged from animal and tracer studies. These data reveal reciprocal (bottom-up and top-down) connections along the ventral and dorsal visual stream (25), including top-down projections from frontal back to early visual cortices (3, 4, 26, 27). To test this signaling hierarchy in humans, we scanned healthy human subjects in two brain states, lying with either eyes closed or eyes open in darkness, and calculated EC using our integrated approach. Consistent with previously reported data, MCM revealed persistent and bidirectional interactions between visual stream areas during both the "eyes closed" and "eyes open" conditions, but frontal top-down modulation of early visual areas only during the eyes open condition.

In the present study, we used FDG to inform undirected FC from fMRI with a directional measure of postsynaptic neuronal activity. Our results indicate that the integrated measure of MCM serves as a proxy for EC in brain states. Our approach might be particularly useful for investigating other signaling hierarchies in higher cognition or in brain disorders involving, e.g., hippocampal-cortical circuits in Alzheimer's disease (28) or frontomidbrain interactions in major depression (29).

Results

We investigated the signaling hierarchy between an early visual area and functional regions across the entire cortex during conditions of eyes closed and eyes open in a three-step procedure. We first identified regions of interest (ROIs) in visual and association cortices, then determined the FC pathways between the early visual ROIs and all other ROIs, and finally integrated voxel FC and FDG values to reveal the directionality of signaling along these functional pathways via MCM.

Regions Belonging to Visual Stream and Prefrontal Association Networks. Using independent component analysis (ICA) of fMRI data, we parcellated the cortex into clusters sharing characteristic temporal BOLD dynamics. Each cluster had to fulfill certain properties with respect to size and stability of occurrence (*Materials and Methods*). We then mapped these clusters onto recently defined networks from a 1,000-subject dataset (Fig. 2, colored outline). Previous work identified two networks (dark violet, green) as part of an extended visual hierarchy and three networks covering prefrontal association areas (30). According to this nomenclature, we identified five ROIs along ventral and dorsal visual streams (Fig. 2, *Left*) and five ROIs in frontal association networks (Fig. 2, *Right*). Table 1 lists all anatomic structures covered by each ROI. We selected the calcarine sulcus (CaS) as the early visual area for all subsequent analyses of FC and MCM, because it fully covers the area of greatest metabolic increase when subjects open their eyes (10) (Fig. 2, *Middle*, blue).

FC Pathways Between Regions. In a second step, we identified FC pathways between the CaS and all other ROIs via pairwise temporal correlations between individual cluster time-series (FC_{cl}) from the ICA. For each subject, we first calculated the FC_{cl} between the CaS and all ROIs of the visual stream and submitted these values to ANOVA with region [striate cortex (StC), extrastriate cortex (ExC), inferior temporal gyrus (ITG), and superior parietal lobe (SPL)] and condition (eyes closed/open) as factors (Fig. 3*A*). We found a main effect for region ($F_{1,21} = 3.41$, $P = 0.02$), but not for condition ($F_{1,21} = 3.27$, $P = 0.075$), and no interaction of region and condition ($F_{3,19} = 2.14$, $P = 0.1$). One-sample t tests, however, showed a positive FC_{cl} between the CaS and each of the visual stream ROIs across both conditions (StC: $t_{21} = 5.72$, $P = 1.1 \times 10^{-5}$; ExC: $t_{21} = 10.06$, $P = 1.7 \times 10^{-9}$;

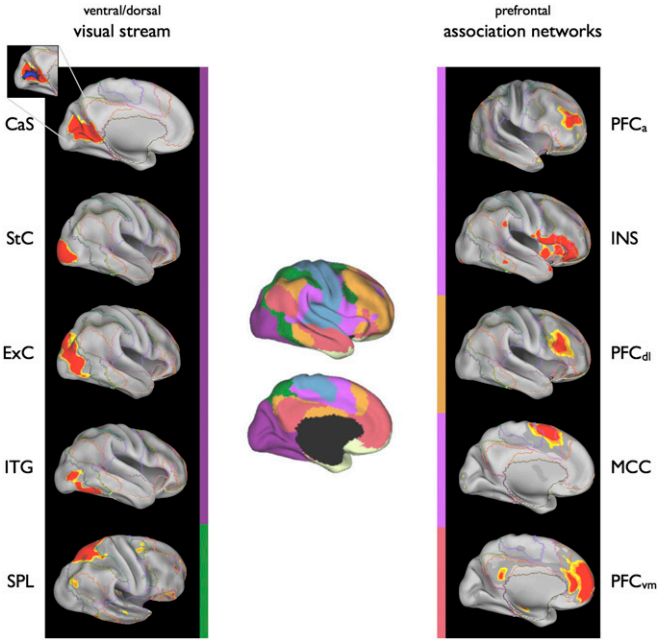

Fig. 2. Brain regions belonging to visual stream and prefrontal association networks. Spatial maps ($P < 0.05$, corrected) are projected onto the inflated cortical surface of a standard brain. Major networks of a recent 1,000-subject analysis are illustrated in the middle panel (top, lateral surface; bottom, medial surface) using different colors and serve as a reference for the assignment of each of our ROIs to its closest match. Reprinted from ref. 30. Ventral/dorsal visual stream ROIs include the CaS, StC, ExC, ITG, and SPL. Prefrontal association network ROIs include the PFC_a, INS, PFC_{dl}, MCC, and PFC_{vm}. Table 1 lists the anatomic structures covered by each ROI. The CaS was chosen as the early visual region for further analyses, because it fully covers the cluster of greatest increase in metabolic activity during the eyes open condition from an earlier analysis (10).

Table 1. Brain regions and associated networks as illustrated in Fig. 2

Label	Anatomy	Network
CaS	Calcarine sulcus	Visual (dark violet)
StC	Striate cortex, lingual gyrus, lateral occipital	Visual (dark violet)
ExC	Extrastriate cortex, inferior parietal	Visual (dark violet)
ITG	Fusiform gyrus, inferior temporal	Visual (dark violet)
SPL	Superior parietal/frontal eye fields	Spatial attention (green)
PFC_a	Anterior prefrontal cortex	Salience (purple)
INS	Insular cortex, frontal operculum	Salience (purple)
PFC_{dl}	Dorsolateral prefrontal cortex	Central executive (yellow)
MCC	Middle cingulate cortex	Salience (purple)
PFC_{vm}	Ventromedial prefrontal cortex	Default mode (red)

ITG: $t_{21} = 6.62$, $P = 1.5 \times 10^{-6}$; SPL: $t_{21} = 8.12$, $P = 5.8 \times 10^{-8}$). Thus, persistent functional pathways between CaS and all regions along the ventral and dorsal visual streams exist during both the eyes closed and eyes open conditions.

Similarly, we tested whether functional pathways exist between the CaS and any prefrontal association region. We calculated the FC_{cl} between the CaS and each frontal ROI and submitted these measures to ANOVA with region [anterior prefrontal cortex (PFC_a), insular cortex (INS), dorsolateral prefrontal cortex (PFC_{dl}), middle cingulate cortex (MCC), and ventromedial prefrontal cortex (PFC_{vm})] and condition (eyes closed/open) as factors. We found main effects for region ($F_{1,21} = 11.1$, $P = 1.7 \times 10^{-7}$) and condition ($F_{1,21} = 19.14$, $P = 3.0 \times 10^{-5}$), along with an interaction of region and condition ($F_{4,18} = 5.54$, $P = 0.0005$). This means that the FC_{cl} between the CaS and prefrontal ROIs strongly differs for selected regions between conditions. Post hoc two-sample t tests evaluating the two-way interaction indicated that the FC_{cl} between the CaS and PFC_a ($t_{21} = 2.58$, $P = 0.02$), INS ($t_{21} = 4.17$, $P = 0.0005$) and MCC ($t_{21} = 4.07$, $P = 0.0006$) increased during the eyes open condition (Fig. 3*B*); interestingly, these three frontal regions all belong to the salience network (shown in purple). Note that only salience regions INS and MCC showed increased FC when using a stringent Bonferroni correction for possibly nine two-sample t tests in this FC analysis. Thus, FC_{cl} between early visual and salience regions increases when subjects open their eyes. On the other hand, we found no difference in or persistent FC_{cl} with the PFC_{dl} ($P > 0.1$) and PFC_{vm} ($P > 0.1$), which belong to the central executive and default mode networks, respectively. Taken together, our FC_{cl} analyses reveal persisting visual pathways across conditions and additional salience pathways once subjects open their eyes.

MCM Reveals EC Between Regions. In a final step, we investigated EC among these visual and salience pathways. Here MCM identifies whether an area receives signaling input, or afferent EC, by integrating voxels' FC and energy metabolism. For a given pathway, e.g., between the CaS and StC, we first used a cluster time course of the CaS to calculate FC_{vox} for each voxel in the StC. The spatial correlation analysis between FC_{vox} and FDG_{vox} then revealed whether the StC receives afferent, or bottom-up, signaling (Fig. 4, red bars). A similar analysis in the CaS tested for the inverse direction, i.e., top-down signaling (Fig. 4, blue bars). Importantly, we performed this integrated analysis on maximally unsmoothed data by omitting spatial normalization or smoothing of both the fMRI and FDG data. This allowed us to calculate the signaling hierarchy in each subject individually. Illustrations of alignment between coregistered EPI and PET images are provided in Fig. S1.

First, we examined the signaling hierarchy along the visual stream pathways. We calculated MCM for all visual ROIs on both eyes closed and eyes open datasets and submitted these measures to ANOVA with region (StC, ExC, ITG, and SPL) and direction (bottom-up/top-down) as factors. We found main effects of region ($F_{1,21} = 3.92$, $P = 0.01$) and direction ($F_{1,21} = 4.62$, $P = 0.033$), along with a two-way interaction between region and direction ($F_{3,19} = 5.21$, $P = 0.002$), indicating that signaling direction differs for only certain pathways. Post hoc t tests evaluating this two-way interaction revealed unidirectional signaling for the SPL pathway ($t_{21} = 4.1$, $P = 0.0002$; $P = 0.001$ Bonferroni-corrected for seven two-sample t tests in MCM analysis), but not for any of the other connections ($P > 0.1$). As shown in Fig. 4*A*, the SPL pathway is driven by top-down signaling (blue bar), whereas communication in all other visual stream pathways is characterized by bidirectional EC.

Similarly, we investigated the EC along the salience pathways during the eyes open condition. In individual subject spaces, we calculated MCM and submitted these measures to ANOVA with region (PFC_a, INS, and MCC) and direction (bottom-up/top-down) as factors. We found a main effect of direction ($F_{1,21} = 41.53$, $P = 4.1 \times 10^{-9}$), but no main effect of region ($P > 0.1$) or any interaction effects ($P > 0.2$). Thus, there is consistent unidirectional communication along the salience pathways. Post hoc t tests revealed that all salience regions exert a top-down influence on the CaS (PFC_a: $t_{21} = 4.78$, $P = 0.0001$; INS: $t_{21} = 3.26$, $P = 0.004$; MCC: $t_{21} = 3.04$, $P = 0.007$; all $P < 0.05$ Bonferroni-corrected) (Fig. 4*B*). Taken together, these MCM values reveal a distinct signaling hierarchy along visual stream and salience pathways. Independent of condition, bidirectional communication occurs between early and higher visual regions, but top-down signaling occurs from a parietal region. Once subjects open their eyes, additional top-down signaling from a salience network occurs.

Finally, in two control analyses, we evaluated the effects of voxel and ROI size on the results of MCM. To diminish the effect of spatial smoothing, which might artificially increase spatial correlations

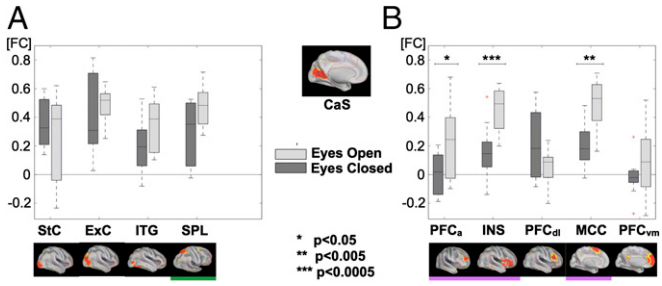

Fig. 3. FC pathways during the eyes closed and eyes open conditions. (*A*) Stable FC is seen between the CaS (image to the right of the graph) and all other visual regions (StC, ExC, ITG, and SPL) independent of condition (results of one-sample t tests; see text). (*B*) FC between the CaS and all regions of the salience network (purple) increases only during the eyes open condition (two-sample t tests; PFC_a: $P < 0.05$; INS: $P < 0.0005$; MCC: $P < 0.005$). The two other regions (PFC_{dl} and PFC_{vm}) show no FC with the CaS ($P > 0.1$). Note that only salience regions INS and MCC show increased FC when a stringent Bonferroni correction is applied for possibly nine two-sample t tests in this FC analysis. Boxplots indicate median, 25th–75th percentiles (box), and extreme data points (whiskers).

NEUROSCIENCE

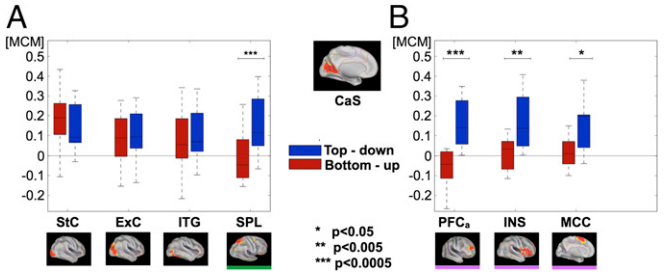

Fig. 4. EC between regions using MCM. (*A*) Stable bidirectional (bottom-up/top-down) signaling between the CaS and all other visual regions (StC, ExC, ITG, and SPL) and top-down modulation from the SPL ($P < 0.0005$) independent of condition. (*B*) All frontal regions of the salience network (purple) exert top-down modulation of the CaS only during the eyes open condition (PFC_a: $P < 0.0005$; INS: $P < 0.005$; MCC: $P < 0.05$). Boxplots indicate median, 25th–75th percentiles (box), and extreme data points (whiskers).

between voxel values, we omitted spatial normalization and smoothing during preprocessing. Nonetheless, spatial sampling and the extent of ROI size in the target area might influence the strength of MCM. Fig. S2 presents MCM data for varying ROI and voxel sizes (Fig. S2*A*), both of which show very consistent results. We found identical directionality with larger voxels (Fig. S2*B*), as well as with smaller target ROIs down to one-quarter of the original ROI size (Fig. S2*C*).

Discussion

Here we have established a new framework for identifying brain state EC from simultaneously acquired fMRI and FDG-PET data. We first characterized functional pathways among visual, parietal, and frontal regions by calculating FC from fMRI data. We then identified the direction of communication among these pathways by integrating neuroenergetics data obtained from FDG-PET. We found permanent and bidirectional communication between early and higher visual regions of the occipital cortex and top-down signaling from parietal regions. Only during the eyes open condition did additional top-down signaling from a frontal salience network emerge. We have identified dynamically changing signaling pathways during simple brain states in humans, offering a method to further investigate directed communication in healthy and diseased brains.

In human brain imaging, the visual networks are among the most consistent networks in FC analyses (30, 31). Our FC analysis revealed functional pathways between the early visual CaS ROI and all ROIs along the ventral and dorsal visual streams, including inferior temporal and parietal regions. These functional pathways were stable across conditions, suggesting interaction between these regions beyond functional processing of visual input, possibly reflecting underlying anatomic connections. In the monkey brain, retrograde tracer studies have shown feedforward and feedback pathways among striate, extrastriate, and parietal regions (4, 26, 27). Structural imaging with diffusion tensor imaging in humans also has identified a strong overlap between FC and anatomic pathways (32). Our FC analysis supports the notion of functionally distinct, yet highly connected, areas along the visual processing stream.

The frontal cortex includes a core set of networks—default mode, central executive, and salience networks—that have been assigned to higher cognitive functions and are prominently affected in neuropsychiatric disorders (13, 33). We evaluated functional pathways between the early visual cortex and all three networks, but identified FC only with regions of the salience network and then only during the eyes open condition. This finding is interesting, because it is consistent with the behavioral relevance ascribed to each network. Current knowledge assigns self-related memory processing to the default mode network (34), event-related and error-based processing to the central executive network (35), and set maintenance or salience processing of internal and external states to the salience network (36). For instance, FC in the salience network correlates with prescan anxiety ratings in humans (37). The switch from eyes closed to eyes open might induce a change in brain state reflected by salience FC and prepare the organism for event- or self-related processing in the central executive and default mode networks once visual input is present.

We next integrated independent voxel measures of FC and FDG to reveal EC along the visual stream and salience pathways. For the visual pathways, we identified bidirectional communication among regions in the occipital cortex and top-down signaling from fronto-parietal regions. Whereas early anatomic studies suggested a bottom-up hierarchy along the visual streams, recent work has stressed the importance of feedback signaling onto early visual areas. The StC receives considerably more feedback and lateral input than feedforward thalamic afferents (27, 38). This is achieved by a dense network of cortico-cortical connections (1), and feedback signaling occurs not only from extrastriate cortices, but also from parietal cortices (39, 40). Direct feedback connections onto V1 have even been shown for the frontal eye fields (4) that we identified as the most frontal region within the dorsal visual stream (SPL). Taken together, our results largely reflect anatomic data from nonhuman primate studies of strong reciprocal connections along the extended visual processing pathway. Our data only indicate the directionality of communication between major hubs of functional networks, however, and we cannot rule out the possibility of intermediate brain regions below the spatial resolution of fMRI that might mediate the influence on early visual areas.

Finally, we also found a top-down influence from all prefrontal regions of the salience network. Again, this communication might occur along downstream regions that we have missed with current human imaging methods. Nonetheless, previous work revealed top-down modulation of visual cortex activity by frontal regions. In humans, inhibitory transcranial magnetic stimulation of the inferior frontal cortex has been shown to decrease the performance of early visual processing (41). Moreover, recent studies in monkeys using novel tracer techniques have identified previously unknown long-range connections between the prefrontal and early visual cortex (42). Our finding of top-down signaling also might reflect a more general notion about the underestimated influence of cortical feedback, particularly onto the early visual cortex (3, 24). A recent study identified twice as many feedback connections as feedforward connections for cortico-cortical pathways, and also showed that feedback connections tend to be more long-range, whereas feedforward pathways are comparatively short-range (26).

Certain methodological factors must be taken into account when interpreting our MCM data. First, our experimental setup has several limitations. The instruction to keep eyes closed or open is easy for subjects to follow, particularly with respect to scanning; however, resting brain states obviously differ across subjects and entail neuronal processes across many cognitive domains that cannot be controlled for. We chose the resting state on the basis of the extensive literature in this area, and because of the self-evident difficulties in designing tasks that engage sustained and consistent processing over extended time periods (necessary to acquire PET data). A positive aspect, however, is the fact that a basic set of networks emerged consistently in the resting state across subjects (43). Our study design also had to accommodate the fact that temporal resolution of PET is limited to one saturated image of accumulated tracer after 30 min of scanning. Although recent fMRI studies suggest temporal variability of FC (i.e., dynamic FC) within and between networks (44), the MCM approach is based on FC expressed (possibly intermittently) consistently over extended periods. This property ensures that the time scale of coupling is commensurate with the time scale of metabolic (PET) measurements. In other words,

MCM pertains to the EC mediating consistent FC that may or may not be fluctuating over time. It might be interesting to revisit this issue by using the average of dynamic FC, as opposed to FC per se. A final limitation of the present study is that interpretation of MCM results might be confounded by varying levels of arousal during the eyes closed and eyes open conditions. In other words, frontal top-down signaling during eyes open might indicate anticipatory signaling from salience regions, or frontal uncoupling during eyes closed may occur simply because subjects have lower levels of arousal.

Second, MCM relies on the assumption that voxel values of FC and FDG spatially correlate with each other in connected regions. Underlying vascular heterogeneity might induce false-positive or -negative spatial correlations, however. In the resting state fMRI literature, the influence of cerebral blood flow (CBF) and vessel size on BOLD-FC is increasingly discussed (45), and recent studies suggest strong BOLD-CBF coupling (46, 47). There is also evidence that these CBF fluctuations indicate reactivity to neuronal activity rather than to heterogeneous vascularity, however. Tak et al. (46) also acquired data on large-vessel volume fraction and found that BOLD-FC was inversely related to macrovascular volume fraction. The stronger relationship with small- to medium-sized vessels (closer to neuronal activity) was particularly prominent for major FC hubs. In summary, spatial variation in neurovascular mechanisms will lead to spatial inhomogeneities in measured BOLD signals that will clearly affect spatial correlation over voxels. To a certain extent, our use of FC (as opposed to BOLD signal per se) mitigates this problem, in the sense that the correlation between the BOLD signals in two regions does not change with their amplitude (e.g., neurovascular sensitivity). This assumes that the signal-to-noise ratio of BOLD time series is spatially invariant, however. If it is not, then MCM may be prone to false-negative results.

As noted by our reviewers, the potentially confounding effects of neurovascular heterogeneity cannot be invoked to explain the condition-specific changes in EC that we observed. This means that the assessment of changes in EC may be more robust to vascular heterogeneity. On the other hand, the combination of two modalities with similar voxel resolution also has distinct advantages with respect to sensitivity. Integrating data acquired simultaneously and independently from the same subject allowed us to avoid spatial distortion of imaging data, which commonly occurs before statistical analysis (48). We omitted spatial normalization to a standard brain and also spatial smoothing as we integrated the two datasets in individual subject space. Moreover, our control analyses showed that MCM was robust against variations in voxel and ROI size. Thus, this approach might prove sufficiently sensitive for even single-subject analyses.

Third, an ongoing discussion in the PET literature surrounds the issue of how to interpret FDG signals. FDG uptake reflects energy consumption and to a large part is related to neuronal signaling (49); however, a critical question is whether neurons themselves or astrocytes consume most of the energy provided by glucose. Numerous studies have provided evidence for both cell types, but a very recent study "identified neurons as the principle locus of glucose uptake as visualized by functional brain imaging" (50). According to that study, FDG-PET is an ideal surrogate for energy consumption in neurons and specifically at synapses. Furthermore, this idea supports the general assumption about the neuronal basis of the BOLD signal. Earlier studies of simultaneous electrophysiology and fMRI have concluded that BOLD signal fluctuations reflect synaptic activity rather than spiking activity (51, 52). Using complementary methods like PET, we can now confirm this assumption directly in humans.

Although we and others found a partial spatial overlap between FDG and fMRI measures in previous studies (10, 53), MCM is a novel approach using energy consumption as a proxy for directional signaling. The question remains as to which aspects of EC (and endogenous fluctuations) best predict metabolic activity as measured by FDG. There are a number of competing hypotheses here. For example, a decrease in regional self-inhibition may correspond to increased excitability and an increase in metabolism (and spatial correlation with FC). Conversely, metabolic increases may be mediated directly by afferent EC from source regions. Finally, the best predictor of metabolic activity may be the amplitude of neuronal fluctuations mediated by changes in EC. In a future study, we will apply stochastic and spectral dynamic causal modeling (DCM) to the data described above (17). The parameters (intrinsic and extrinsic connectivity) and the amplitude of inferred neuronal fluctuations will be used to predict regional metabolism (and its spatial correlation with FC) to identify the key determinants that underlie MCM. The use of spectral DCM here may be interesting, because this approach explicitly parameterizes the spectral profile of endogenous neuronal fluctuations, aa well as their implicit time constants. We hope to test the hypothesis that the determinants of MCM rely not just on the amplitude of neuronal fluctuations (mediated by EC), but also on the characteristic time constants as modeled with power law scaling.

Materials and Methods

Our analysis was performed on 24 healthy subjects (16 males, 8 females; average age, 54.7 ± 9.9 y; all right-handed) participating in a simultaneous FDG-PET/fMRI brain imaging study. All participants gave informed consent to procedures approved by the Ethics Review Board of the Klinikum Rechts der Isar, Technische Universität München. Scanning was performed on an integrated Siemens Biograph mMR scanner capable of simultaneously acquiring PET and MRI (3 T) data using the vendor-supplied 12-channel phase-array head coil.

We simultaneously measured FDG-PET activity and BOLD-fMRI signals during resting conditions of either eyes closed (CLOSED) or eyes open (OPEN) during the initial 10 min immediately after bolus injection of FDG tracer. At 30 min postinjection, we recorded the saturated list mode PET dataset for 10 min. All scanning was performed in a dimmed environment obtained by switching off all lights, including those in the scanner bore. Subjects were instructed to keep their eyes closed/open, to relax, to not think of anything in particular, and to not fall asleep. We assessed each subject's level of arousal and anxiety using the State Trait Anxiety Inventory before the start of the scanning session (CLOSED/OPEN: 35.5 ± 6.9/30.8 ± 5.6; $P = 0.18$), and measured blood pressure and venous glucose level (<140 mg/dL in all subjects).

We applied two different preprocessing pipelines for the initial FC analysis of fMRI data, and for the final integrated MCM analysis of fMRI and PET data in single-subject space.

FC Analysis. We first identified ROIs according to a standard set of networks that Yeo et al. (30) recently established in a 1,000-subject dataset. We followed our previous processing pipeline for ICA of fMRI data (54). We applied slice-time correction, realignment, normalization to a standard template, and spatial smoothing using a Gaussian kernel with an FWHM of 6 mm. We then subjected the concatenated data of all subjects to a group ICA using GIFT (Medical Imaging Analysis Lab, The Mind Research Network) and identified 70 spatially independent components (ICs) with corresponding signal time series (31). Only the most stable ICs with a stability index > 0.9 were identified by iteratively running 30 ICAs using the ICASSO procedure (55). We automatically selected ICs as relevant ROIs by running spatial regression against the spatial maps of the seven-network decomposition from Yeo et al. (30). Finally, we identified functional pathways of FC between an early visual area (CaS) and all other visual stream ROIs (StC, ExC, and ITG, SPL) and prefrontal association ROIs (PFC_a, INS, PFC_{dl}, MCC, and PFC_{vm}). For each subject separately, we calculated the temporal Pearson's correlation between the cluster time series of the CaS and that of all other ROIs.

Multimodal MCM Analysis in Single-Subject Space. In this analysis, we integrated voxel-wise measures of FC and FDG activity in single-subject spaces to reveal EC among previously established FC pathways. We used the temporally (slice time corrected) and spatially corrected EPI volumes of each subject, but omitted normalization and smoothing procedures to achieve the least distorted volumes. We then coregistered the mean FDG-PET volume to the mean EPI volume, scaled PET data to normalized FDG activity by whole-brain FDG uptake values, and resampled both datasets to common voxel dimensions of $2 \times 2 \times 2$ mm^3. We then submitted the fMRI and FDG-PET data to a two-step procedure to calculate MCM (Fig. 1).

Based on the energy model of neuronal signaling, a positive spatial correlation between the voxel profiles of FC (FC_{vox}) and FDG activity (FDG_{vox})

identifies a region as the input area of a pathway. FDG_{vox} is derived from FDG activity maps, and FC_{vox} is calculated as the temporal correlation between each voxel time series within the (target) ROI and the cluster time series of the connected (seed) region, i.e., FC_{vox} in the StC with cluster time series of the CaS. The spatial extent of each ROI was defined by the initial ICA maps ($z > 3$) back-projected into individual space.

More detailed information is provided in *SI Materials and Methods*.

ACKNOWLEDGMENTS. We thank Edward Bullmore for discussions during the process of data analysis. We also thank our colleagues at the Technische Universitaet Muenchen, particularly Claus Zimmer, Markus Schwaiger, Igor Yakushev, Anne Winter, Sylvia Schachoff, Brigitte Dzewas, Michael Herz, and Mathias Lukas. This work was supported by a university grant from the Kommission fuer klinische Forschung (Grant 8762754, to V.R. and A.D.) at the Klinikum Rechts der Isar der Technischen Universitaet Muenchen.

1. Felleman DJ, Van Essen DC (1991) Distributed hierarchical processing in the primate cerebral cortex. *Cereb Cortex* 1(1):1–47.
2. Goldman-Rakic PS (1988) Topography of cognition: Parallel distributed networks in primate association cortex. *Annu Rev Neurosci* 11(1):137–156.
3. Gilbert CD, Li W (2013) Top-down influences on visual processing. *Nat Rev Neurosci* 14(5):350–363.
4. Clavagnier S, Falchier A, Kennedy H (2004) Long-distance feedback projections to area V1: Implications for multisensory integration, spatial awareness, and visual consciousness. *Cogn Affect Behav Neurosci* 4(2):117–126.
5. Bressler SL, Menon V (2010) Large-scale brain networks in cognition: Emerging methods and principles. *Trends Cogn Sci* 14(6):277–290.
6. Fox MD, Raichle ME (2007) Spontaneous fluctuations in brain activity observed with functional magnetic resonance imaging. *Nat Rev Neurosci* 8(9):700–711.
7. Lewis CM, Baldassarre A, Committeri G, Romani GL, Corbetta M (2009) Learning sculpts the spontaneous activity of the resting human brain. *Proc Natl Acad Sci USA* 106(41):17558–17563.
8. Albert NB, Robertson EM, Miall RC (2009) The resting human brain and motor learning. *Curr Biol* 19(12):1023–1027.
9. van Kesteren MTR, Fernández G, Norris DG, Hermans EJ (2010) Persistent schema-dependent hippocampal–neocortical connectivity during memory encoding and postencoding rest in humans. *Proc Natl Acad Sci USA* 107(16):7550–7555.
10. Riedl V, et al. (2011) Repeated pain induces adaptations of intrinsic brain activity to reflect past and predict future pain. *NeuroImage* 57(1):206–213.
11. Hampson M, Driesen NR, Skudlarski P, Gore JC, Constable RT (2006) Brain connectivity related to working memory performance. *J Neurosci* 26(51):13338–13343.
12. Harmelech T, Preminger S, Wertman E, Malach R (2013) The day-after effect: Long-term, Hebbian-like restructuring of resting-state fMRI patterns induced by a single epoch of cortical activation. *J Neurosci* 33(22):9488–9497.
13. Menon V (2011) Large-scale brain networks and psychopathology: A unifying triple network model. *Trends Cogn Sci* 15(10):483–506.
14. Greicius M (2008) Resting-state functional connectivity in neuropsychiatric disorders. *Curr Opin Neurol* 21(4):424–430.
15. Friston KJ (2011) Functional and effective connectivity: A review. *Brain Connect* 1(1): 13–36.
16. Bastos-Leite AJ, et al. (2015) Dysconnectivity within the default mode in first-episode schizophrenia: A stochastic dynamic causal modeling study with functional magnetic resonance imaging. *Schizophr Bull* 41(1):144–153.
17. Friston KJ, Kahan J, Biswal B, Razi A (2014) A DCM for resting-state fMRI. *Neuroimage* 94:396–407.
18. Hyder F, Rothman DL, Bennett MR (2013) Cortical energy demands of signaling and nonsignaling components in brain are conserved across mammalian species and activity levels. *Proc Natl Acad Sci USA* 110(9):3549–3554.
19. Attwell D, Laughlin SB (2001) An energy budget for signaling in the grey matter of the brain. *J Cereb Blood Flow Metab* 21(10):1133–1145.
20. Attwell D, Iadecola C (2002) The neural basis of functional brain imaging signals. *Trends Neurosci* 25(12):621–625.
21. Alle H, Roth A, Geiger JRP (2009) Energy-efficient action potentials in hippocampal mossy fibers. *Science* 325(5946):1405–1408.
22. Harris JJ, Jolivet R, Attwell D (2012) Synaptic energy use and supply. *Neuron* 75(5): 762–777.
23. Jao T, et al. (2013) Volitional eyes opening perturbs brain dynamics and functional connectivity regardless of light input. *Neuroimage* 69:21–34.
24. Anderson JC, Kennedy H, Martin KAC (2011) Pathways of attention: Synaptic relationships of frontal eye field to V4, lateral intraparietal cortex, and area 46 in macaque monkey. *J Neurosci* 31(30):10872–10881.
25. Mishkin M, Ungerleider LG, Macko KA (1983) Object vision and spatial vision: Two cortical pathways. *Trends Neurosci* 6:414–417.
26. Markov NT, et al. (2014) Anatomy of hierarchy: Feedforward and feedback pathways in macaque visual cortex. *J Comp Neurol* 522(1):225–259.
27. Muckli L, Petro LS (2013) Network interactions: Non-geniculate input to V1. *Curr Opin Neurobiol* 23(2):195–201.
28. Pasquini L, et al. (2015) Link between hippocampus' raised local and eased global intrinsic connectivity in AD. *Alzheimers Dement* 11(5):475–484.
29. Lui S, et al. (2011) Resting-state functional connectivity in treatment-resistant depression. *Am J Psychiatry* 168(6):642–648.
30. Yeo BTT, et al. (2011) The organization of the human cerebral cortex estimated by intrinsic functional connectivity. *J Neurophysiol* 106(3):1125–1165.
31. Allen EA, et al. (2011) A baseline for the multivariate comparison of resting-state networks. *Front Syst Neurosci* 5:2.
32. Honey CJ, Kötter R, Breakspear M, Sporns O (2007) Network structure of cerebral cortex shapes functional connectivity on multiple time scales. *Proc Natl Acad Sci USA* 104(24):10240–10245.
33. Chen AC, et al. (2013) Causal interactions between fronto-parietal central executive and default-mode networks in humans. *Proc Natl Acad Sci USA* 110(49):19944–19949.
34. Andrews-Hanna JR, Reidler JS, Sepulcre J, Poulin R, Buckner RL (2010) Functional-anatomic fractionation of the brain's default network. *Neuron* 65(4):550–562.
35. Dosenbach NUF, Fair DA, Cohen AL, Schlaggar BL, Petersen SE (2008) A dual-networks architecture of top-down control. *Trends Cogn Sci* 12(3):99–105.
36. Menon V, Uddin LQ (2010) Saliency, switching, attention and control: A network model of insula function. *Brain Struct Funct* 214(5-6):655–667.
37. Seeley WW, et al. (2007) Dissociable intrinsic connectivity networks for salience processing and executive control. *J Neurosci* 27(9):2349–2356.
38. Budd JM (1998) Extrastriate feedback to primary visual cortex in primates: A quantitative analysis of connectivity. *Proc Biol Sci* 265(1400):1037–1044.
39. Barone P, Batardiere A, Knoblauch K, Kennedy H (2000) Laminar distribution of neurons in extrastriate areas projecting to visual areas V1 and V4 correlates with the hierarchical rank and indicates the operation of a distance rule. *J Neurosci* 20(9): 3263–3281.
40. Lewis JW, Van Essen DC (2000) Corticocortical connections of visual, sensorimotor, and multimodal processing areas in the parietal lobe of the macaque monkey. *J Comp Neurol* 428(1):112–137.
41. Zanto TP, Rubens MT, Thangavel A, Gazzaley A (2011) Causal role of the prefrontal cortex in top-down modulation of visual processing and working memory. *Nat Neurosci* 14(5):656–661.
42. Markov NT, et al. (2013) The role of long-range connections on the specificity of the macaque interareal cortical network. *Proc Natl Acad Sci USA* 110(13):5187–5192.
43. Biswal BB, et al. (2010) Toward discovery science of human brain function. *Proc Natl Acad Sci USA* 107(10):4734–4739.
44. Allen EA, et al. (2014) Tracking whole-brain connectivity dynamics in the resting state. *Cereb Cortex* 24(3):663–676.
45. Liu TT (2013) Neurovascular factors in resting-state functional MRI. *Neuroimage* 80: 339–348.
46. Tak S, Polimeni JR, Wang DJJ, Yan L, Chen JJ (2015) Associations of resting-state fMRI functional connectivity with flow-BOLD coupling and regional vasculature. *Brain Connect* 5(3):137–146.
47. Liang X, Zou Q, He Y, Yang Y (2013) Coupling of functional connectivity and regional cerebral blood flow reveals a physiological basis for network hubs of the human brain. *Proc Natl Acad Sci USA* 110(5):1929–1934.
48. Shaw ME, et al. (2003) Evaluating subject specific preprocessing choices in multi-subject fMRI data sets using data-driven performance metrics. *Neuroimage* 19(3): 988–1001.
49. Raichle ME (2009) A brief history of human brain mapping. *Trends Neurosci* 32(2):118–126.
50. Lundgaard I, et al. (2015) Direct neuronal glucose uptake heralds activity-dependent increases in cerebral metabolism. *Nat Commun* 6:6807.
51. Viswanathan A, Freeman RD (2007) Neurometabolic coupling in cerebral cortex reflects synaptic more than spiking activity. *Nat Neurosci* 10(10):1308–1312.
52. Logothetis NK, Pauls J, Augath M, Trinath T, Oeltermann A (2001) Neurophysiological investigation of the basis of the fMRI signal. *Nature* 412(6843):150–157.
53. Tomasi D, Wang G-J, Volkow ND (2013) Energetic cost of brain functional connectivity. *Proc Natl Acad Sci USA* 110(33):13642–13647.
54. Dovern A, et al. (2012) Intrinsic network connectivity reflects consistency of synesthetic experiences. *J Neurosci* 32(22):7614–7621.
55. Himberg J, Hyvärinen A, Esposito F (2004) Validating the independent components of neuroimaging time series via clustering and visualization. *Neuroimage* 22(3):1214–1222.
56. Tagliazucchi E, et al. (2012) Automatic sleep staging using fMRI functional connectivity data. *Neuroimage* 63(1):63–72.
57. Fox PT, Raichle ME, Mintun MA, Dence C (1988) Nonoxidative glucose consumption during focal physiologic neural activity. *Science* 241(4864):462–464.
58. Drzezga A, et al. (2011) Neuronal dysfunction and disconnection of cortical hubs in non-demented subjects with elevated amyloid burden. *Brain* 134(Pt 6):1635–1646.
59. Vlassenko AG, Rundle MM, Mintun MA (2006) Human brain glucose metabolism may evolve during activation: findings from a modified FDG PET paradigm. *Neuroimage* 33(4):1036–1041.
60. Calhoun VD, Adali T, Pearlson GD, Pekar JJ (2001) A method for making group inferences from functional MRI data using independent component analysis. *Hum Brain Mapp* 14(3):140–151.
61. Erhardt EB, et al. (2011) Comparison of multi-subject ICA methods for analysis of fMRI data. *Hum Brain Mapp* 32(12):2075–2095.